NuRD independent Mi-2 activity represses ectopic gene expression during neuronal maturation.

Gabriel N Aughey‡, Elhana Forsberg†, Krista Grimes†, Shen Zhang†, Tony D Southall*

†Equal contribution

*Correspondence to t.southall@imperial.ac.uk

Department of Life Sciences, Imperial College London, Sir Ernst Chain Building, London, UK

‡Current address: Department of Clinical and Experimental Epilepsy, UCL Queen Square Institute of Neurology, London, United Kingdom.

Abstract

During neuronal development, extensive changes to chromatin states occur to regulate lineage-specific gene expression. The molecular factors underlying the repression of non-neuronal genes in differentiated neurons are poorly characterised. The Mi2/NuRD complex is a multiprotein complex with nucleosome remodelling and histone deacetylase activity. Whilst NuRD has previously been implicated in the development of nervous system tissues the precise nature of the gene expression programmes that it coordinates are ill-defined. Furthermore, evidence from several species suggests that Mi-2 may be incorporated into multiple complexes that may not possess histone deacetylase activity. Here, we show that Mi-2 activity is required for suppressing the ectopic expression of germline genes in neurons independently of HDAC1/NuRD, whilst components of the NuRD complex including Mi-2 regulate neural gene expression to ensure proper development of the larval nervous system. We find that Mi-2 binding in the genome is dynamic during neuronal maturation and Mi-2 mediated repression of ectopic gene expression is restricted to the early stages of neuronal development, indicating that Mi-2/NuRD is required for establishing stable neuronal transcriptomes during the early stages of neuronal differentiation.

Introduction

Neuronal development involves the transition of multipotent precursor cells into highly specialised neurons with distinct morphological and biochemical characteristics. Extensive gene expression changes accompany the differentiation of precursors into specialised cell-types. These gene expression changes are underpinned by a dynamic chromatin environment in which regulation of nucleosome positioning and histone modifications ensures appropriate transcriptional responses. Whilst recent studies have provided illuminating descriptions of changes to chromatin accessibility and histone modifications during the process of neuronal differentiation (Aughey et al., 2018; Janssens et al., 2022; Preissl et al., 2018; Ziffra et al., 2021), the chromatin-interacting complexes that affect these changes are not well defined.

The Mi-2/NuRD complex is a multiprotein chromatin remodelling complex that influences gene expression via two separate enzymatic activities; ATP-dependent nucleosome remodelling, and histone deacetylation (Tong et al., 1998; Wade et al., 1998; Xue et al., 1998; Zhang et al., 1998). These activities are mediated by enzymes found in two distinct subcomplexes. The nucleosome remodelling subcomplex contains Mi-2 – a well conserved ATP-dependent nucleosome remodeller (CHD4 in mammals). The second subcomplex is characterised by its histone deacetylase activity. NuRD components are widely conserved and broadly expressed in most metazoan tissues, reflecting the important role of the complex in gene regulation. NuRD has been reported to have critical roles in developmental processes, (e.g, in muscle (Gomez-Del Arco et al., 2016) and hematopoietic (Yoshida et al., 2008) cell differentiation), as well as regulation of pluripotent cell reprogramming (Rais et al., 2013).

Mi-2/NuRD complexes have critical roles in neurodevelopment and have been implicated in the aetiology of neurodevelopmental disorders (Hoffmann and Spengler, 2019). A recent study showed that Mi-2 is required in *Drosophila* neuronal lineages to deactivate notch responsive stem-cell enhancers in neuronal progeny, thereby ensuring the fidelity of differentiated cell fate in neurons (Zacharioudaki et al., 2019). Similarly, NuRD was shown to deactivate gene expression by acting on promoters of presynaptic genes to promote synaptic connectivity (Yamada et al., 2014). These studies suggest a predominantly suppressive role for NuRD in the regulation of gene expression. Whilst this is consistent with early models of NuRD activity as a repressive complex, more recent studies have presented a more nuanced role for NuRD in modulating gene expression, which may be neither activating or repressive, but acting to fine tune gene expression and reduce transcriptional noise (Bornelov et al., 2018; Burgold et al., 2019; Ragheb et al., 2020). Therefore, an important unanswered question is whether NuRD is primarily repressive in neuronal development, or whether it may facilitate control of active gene expression as demonstrated in stem cell models.

NuRD composition is dynamic in mouse cortical development, with alternate Mi-2/CHD paralogues incorporated to mediate distinct effects in different developmental stages (Nitarska et al., 2016). In *Drosophila* the components of the NuRD complex are well conserved, (although only single homologues of most NuRD proteins are identified). However, despite the strong conservation of NuRD constituent proteins, and ample evidence for physical interactions between them (Reddy et al., 2010; Zhang et al., 2016), the extent to which the canonical NuRD complex regulates gene expression in *Drosophila* is uncertain. A complex consisting of only Mi2 and MEP-1 (termed dMec), has been suggested to be more prevalent than NuRD in fly, and that this complex is responsible for the majority of Mi-2 dependent phenotypes (Kunert et al., 2009). This observation has not been corroborated by further studies, however, NuRD-independent roles for Mi-2 may be present in human cells (Amaya et al., 2013). Alternatively, it is possible that since NuRD is comprised of pre-assembled modules (Zhang et al., 2016), and Mi-2 may exist as a peripheral component to the core complex (Low et al., 2016), the detection of non-NuRD associated Mi-2 may simply be a proteomic artefact that does not reflect a *bona fide* biological

activity. Therefore, the functional role of dMEC, and its relationship to the canonical NuRD holocomplex, remains poorly characterised.

Here, we set out to better understand the influence of Mi-2/NuRD complex on gene expression in the development of the central nervous system. We find that knockdown of Mi-2 in larval neurons results in ectopic expression non-neuronal genes as well as defective optic lobe development . We show that Mi-2 represses lineage-inappropriate gene expression independently of NuRD, whilst optic lobe phenotypes are phenocopied by other members of the NuRD complex. Genomic profiling with Targeted DamID revealed distinct binding of Mi-2 containing complexes indicating a repressive role for Mi-2 outside of the canonical NuRD complex. We find that Mi-2 is not required for repression of non-neuronal genes after the early stages of differentiation, indicating that Mi-2 activity is critical for ensuring maintenance of the neuronal gene expression programme during maturation, but alternative mechanisms may be employed in fully differentiated neurons.

Results

Mi-2 is required in neurons for survival and larval locomotion.

Mi-2 has been shown to protect neural lineages from mitogenic notch signalling, indicating that NuRD has an important role in gene regulation in the neuroblasts and early progeny of *Drosophila* central nervous system (CNS) lineages. To better understand NuRD function in the fly CNS, we set out to examine the distribution of the core ATP-dependent nucleosome remodelling subunit Mi-2. We utilised a MiMIC insertion line in which Mi-2 is EGFP-tagged at its endogenous locus (*Mi-2-GFP* hereafter). We observed widespread Mi-2 expression with detectable EGFP signal in multiple cell-types in the third instar CNS (Figure 1A). EGFP signal was visible in nuclei of neural stem cells (NSCs) (as distinguished by their larger size and absence of Elav or Repo) as well as all neurons and some glia, (Figure 1A). The nuclear expression of Mi-2 in progenitor and post-mitotic cell-types in the larval CNS suggests that Mi-2 activity is likely to be involved in gene regulation in all stages of neuronal differentiation, including differentiated neurons.

To understand the importance of *Mi-2* expression in neurons, we used RNAi interference (RNAi) to induce cell-type specific knockdown of *Mi-2* in the CNS. An RNAi line targeting Mi-2 was previously shown to produce robust knockdown of Mi-2 in neuronal lineages, therefore, we decided to utilise this line for our study (Zacharioudaki et al., 2019). Using the pan-neuronal *elav*-GAL4 driver we observed lethality during late larval/pupal stages (Figure 1B). Whilst neuronal *Mi-2* appeared dispensable for embryogenesis and larval survival (possibly due to maternal contribution of Mi-2), we observed a severe mobility defect in larval crawling compared to controls (Figure 1C) indicating that *Mi-2* activity in neurons is required throughout development at all life-stages for normal neuronal function.

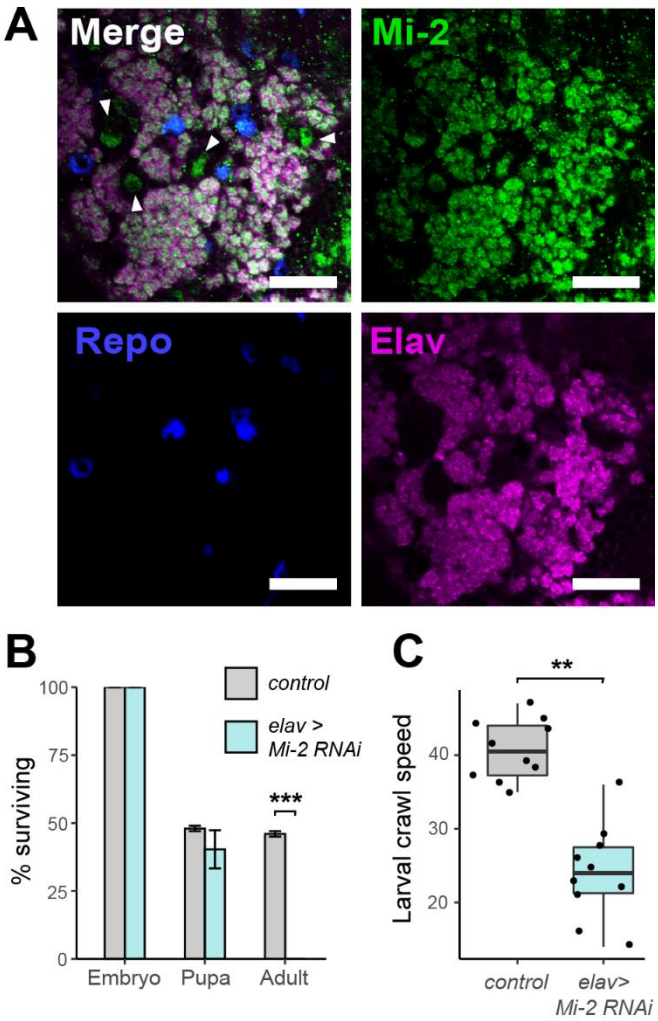

Figure 1. Critical role of Mi-2 in *Drosophila* neurons. A) Third instar larval CNS of *Mi-2* GFP-trap line (scale bar = 20 µm). White arrows highlight NSC nuclei. B) Survival of *Mi-2* RNAi and control (*mCherry-RNAi*) flies during development (100 embryos for each group) **** p < 0.001* (Student's t-test) Represented as mean ± SEM. C) Larval crawl speed (cm/minute) in *Mi-2* RNAi and *mCherry* RNAi controls (n= 10 for each group) *** p < 0.01* (Student's t-test). Represented as a box plot.

111

112 **Mi-2 association with chromatin reveals the presence of distinct complexes**

113 Our data, along with previous reports, suggest that Mi-2/NuRD has an essential role in the regulation
114 of neuronal gene expression. However, it is unclear which genes Mi-2 regulates and whether its function
115 is predominantly via NuRD or dMEC (Mi-2 and MEP-1 only). To better understand NuRD function in
116 regulating neuronal gene expression, we profiled the genomic binding of NuRD complex components
117 using Targeted DamID (TaDa) (Southall et al., 2013). This approach involves fusing a protein of interest
118 to Dam methylase and expressing in a defined cell population, followed by enrichment and sequencing
119 of selectively methylated regions which reflect loci at which the protein associates with DNA (reviewed
120 in (Aughey et al., 2018).

121 We used Targeted DamID to profile genomic association of Mi-2 as well as NuRD components MTA1-
122 like and HDAC1 in neurons (defined by *elav*-GAL4 expression) in the larval CNS. MTA1-like is a core
123 component of the NuRD histone deacetylase subcomplex, with cells lacking MTA orthologues in
124 mammals considered to be effectively NuRD-null (Burgold et al., 2019), whilst HDAC1 is the histone
125 deacetylase subunit (also known as Rpd3). We also assayed for genomic binding of MEP-1, previously
126 reported to associate exclusively with Mi-2 as part of both the dMEC and NuRD complexes. Principal

component analysis revealed a single cluster including both Mi-2 and MEP-1 replicates, whilst the remaining NuRD components, MTA1-like and HDAC1, appeared to be distinct (Figure 2A, B and D). Similarity between Mi-2 and MEP-1 binding is further supported by the close correlation between the two datasets (pearson R^2 = 0.94/0.95), which is almost as strong as that seen between replicates (Appendix Figure 1). In contrast, both MTA-1like and HDAC1 showed relatively poor correlations to MEP-1 or Mi-2, whereas their correlation with each other was slightly stronger. Whilst HDAC1 binding may be expected to be poorly correlated with Mi-2 due to the inclusion of HDAC1 in protein complexes other than NuRD (e.g. with Polycomb Group proteins (Tie et al., 2001)), the relatively low correlation with MTA1-like points towards the possibility of distinct Mi-2 containing complexes having distinct binding in neurons.

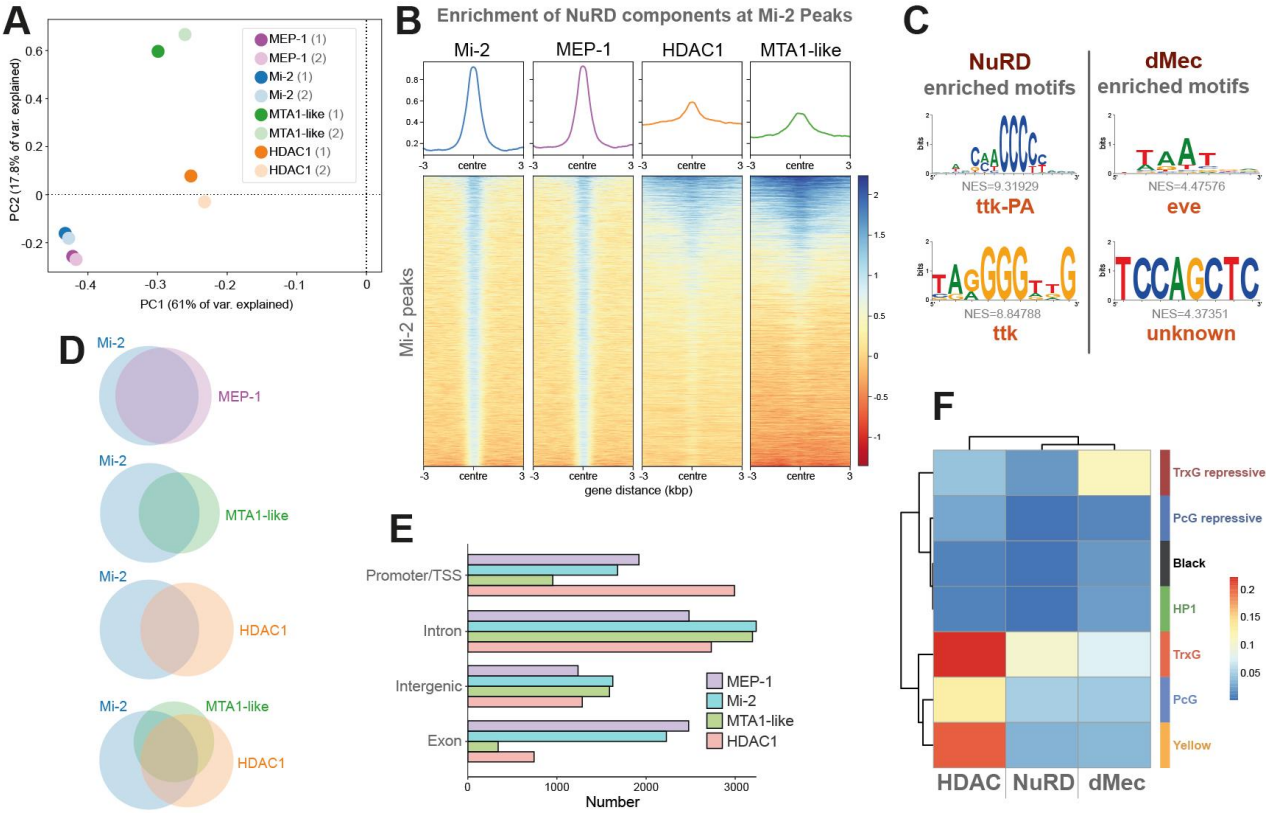

Figure 2. Genomic binding of NuRD components A) Principal component analysis of all NuRD component binding in neurons including replicates. Mi-2/MEP-1 (blue/purple) cluster independently of MTA1-like (green) and HDAC1 (orange) reflecting greater similarity in their binding profiles. B) Heatmap and enrichment plots indicating binding at Mi-2 peaks. C) Top enriched motifs at NuRD and dMec peaks. D) Venn diagrams indicating the number of overlapping peaks between NuRD subunits. All intersections between peaks occur at statistically significant frequencies (Fisher's exact test $p < 10^{-24}$). E) Peak annotation for Mi-2, MEP-1, MTA-1like and HDAC1 peaks. G) Heatmap indicating jaccard similarity statistic between chromatin states and NuRD peaks (Mi-2, MEP-1, MTA-1like and HDAC1) and dMEC (Mi-2 and MEP-1 only), or HDAC1 peaks.

To further understand the relationship between Mi-2 and other NuRD components at the chromatin level, Mi-2 significantly bound peaks were compared to those of MEP-1, MTA1-like and HDAC1. We found that the majority of MTA1-like peaks coincided with Mi-2, although a significant number of Mi-2 peaks did not overlap with MTA1-like (Figure 2D). We observed strong binding of HDAC1 throughout the genome, however, a relatively low proportion of HDAC1 peaks intersected with Mi-2 peaks (Figure 2B, D), indicating that Mi-2 is found in association with chromatin without HDAC1 or MTA1-like at the majority of loci.

We observed that around half of Mi-2 peaks coincided with either MTA1-like or HDAC1 with fewer still having all three detected at the same site (around a quarter of total Mi-2 peaks). We also saw that a smaller proportion of HDAC1 peaks were shared with Mi-2 compared to MTA1-like presumably due to the inclusion of HDAC1 in other chromatin modifying complexes (Figure 2D). We also observed some MTA1-like peaks that did not overlap with Mi-2 or HDAC1, suggesting that MTA1-like may have undefined roles outside of NuRD. As previously indicated, MEP-1 and Mi-2 peaks intersected at almost all loci. Inspection of the genomic features at which the various peaks were found to bind demonstrated further disparity between Mi-2/MEP-1 and MTA1-like/HDAC1. We found that whilst HDAC1 was found to be enriched at promoters and TSS, Mi-2 and MEP-1 were comparatively enriched in gene bodies, particularly in exons (Figure 2E). Together these data suggest that multiple Mi-2 containing complexes interact with chromatin in neurons, that may or may not possess histone deacetylase activity. In line with previous reports, we refer to sites bound by Mi-2 and MEP-1 as "dMEC" hereafter (Kunert et al., 2009), whilst sites with significant binding of all four profiled components are considered "NuRD" target sites.

dMec and NuRD regulate different genes in neuronal differentiation.

Examining the gene ontology (GO) enrichment of genes bound by either NuRD or dMec revealed clear differences in the processes that were regulated by each complex. We found that NuRD-regulated genes were enriched for GO terms related to organismal development, with "central nervous system development" amongst the top enriched terms. In contrast, genes with dMec peaks were enriched for terms relating to cilia function (Appendix Figure 2) reflecting the prevalence of genes that are usually enriched in testis and not expressed in the CNS (although it should be noted that it is possible that some of these genes may also be expressed in fully differentiated sensory neurons). Terms relating to synaptic function were also enriched for genes bound by dMec, which may be expected of a group of genes the expression of which is regulated in neurons. However, inspection of the genes comprising these categories reveals that many of these genes are expressed post-synaptically outside the CNS (*GluRIIA, GluRIIC*) or in later stage pupal CNS in which neurons are in a more differentiated state (e.g. *slo, Syt12*). These results are consistent with a model in which dMEC is largely responsible for repression of gene expression, whilst NuRD is involved in coordinating appropriate transcription of neuronal genes.

175 We examined NuRD and dMec bound sequences for enrichment of sequence motifs to see if we could
176 identify potential cofactors that may be involved in recruitment or regulation of these complexes. For
177 sequences bound by NuRD, we found that the most highly enriched sequence motifs corresponded well
178 to the consensus sequences for *tramtrack* (*ttk*) (Figure 2C). ttk has previously been shown to interact
179 with MEP-1 to recruit the NuRD complex (Reddy et al., 2010), and physical interactions with other NuRD
180 components have also been reported (Rhee et al., 2014). In contrast, the *ttk* motif was not enriched for
181 sequences covered by dMec peaks. Instead, the most highly enriched motif identified was a Hox-like
182 motif corresponding most closely to the transcriptional repressor *even-skipped* (*eve*). The differences in
183 the underlying sequences present at NuRD and non-NuRD Mi-2 binding sites suggest that these
184 complexes maybe recruited to target loci by distinct molecular factors.

185 To gain further insight into how Mi-2 containing complexes regulated gene expression we compared
186 binding to the state of the underlying chromatin. Chromatin can be grouped into discrete states
187 reflecting the occupancy of key regulatory proteins (Filion et al., 2010). We compared the binding of
188 HDAC1, Mi-2, MEP-1 and MTA1-like with published data describing chromatin state domains based on
189 a seven-state model (Marshall and Brand, 2017). We found that HDAC1 binding was associated with
190 broadly permissive chromatin states (Figure 2F). Whilst histone deacetylase activity has been thought
191 to be associated with repression of gene expression, these observations are consistent with previous
192 reports that have described enrichment of HDAC1 binding at active promoters (Wang et al., 2009).
193 Indeed, we also observe strong enrichment of HDAC1 binding at transcription start sites (TSS) as
194 previously reported (Appendix Figure 3). In contrast, Mi-2, MEP-1 and MTA1-like were found to be
195 associated with a mixture of permissive and repressive states, in particular with Trithorax-like
196 permissive and repressive states (Trx-G / Trx-G_repressive). Taking into consideration only regions that
197 are bound by either Mi-2/MEP-1 (dMec), HDAC1 alone, or all four proteins (i.e. NuRD), we saw that
198 whilst NuRD showed the greatest similarity to the Trithorax-like permissive state, Mi2/dMec more
199 strongly coincided with the transcriptionally silent Trithorax-associated repressive state, which is
200 characterised by the presence of Brahma as well as H1 linker histone. These observations support a
201 model in which NuRD independent Mi-2 binding largely mediates gene silencing/repression, whilst
202 NuRD is involved in the regulation of actively expressed genes.

203

204 ***Mi-2* knockdown results in misexpression of non-CNS genes.**

205 To determine the effect of Mi-2 loss on gene expression in neurons of the developing CNS, we performed
206 RNA-seq on larval CNS in which *Mi-2* had been knocked down in neurons by RNAi, and compared to
207 controls in which RNAi targeting mCherry was expressed using the same *elav*-GAL4 driver. We found
208 good correlation between replicates (Appendix Figure 4A, B) and observed that the expression of *Mi-2*
209 itself was found to be significantly downregulated (Appendix Figure 4C) in agreement with previous
210 studies (Zacharioudaki et al., 2019). We found that knockdown of *Mi-2* resulted in significantly more

211 upregulated genes than downregulated (397 downregulated vs 1467 upregulated) indicating that in the
212 context of developing neurons, *Mi-2* has a significant role in the repression of gene expression (Figure
213 3A-C). Gene ontology (GO) analysis of these significantly up-regulated genes revealed enrichment of GO-
214 terms that may be associated with neuronal maturation or function, such as "ion transport", "sensory
215 perception" and "cell projection assembly" (Figure 3E). However, we also saw enrichment for
216 unexpected terms such as "cilium assembly" that are not typically associated with nervous system
217 development or function.

218 Closer inspection of the top up-regulated genes revealed the presence of ectopically expressed genes
219 that are usually expressed in non-CNS tissues such as the germline. For example, *vasa* (*vas,* a well-
220 characterised ovarian germline marker) expression was (~3.5 log2 fold-change) increased compared to
221 controls (Figure 3B). Similarly, *gammaTub37C* – a female germline specific isoform of tubulin, was also
222 very highly upregulated (Figure 3A and Figure EV1A, C), as well as *RpS5b*, encoding a germline specific
223 ribosomal protein (Figure EV1B, C). We also saw evidence of male-germline specific genes being
224 upregulated, for example *CG15446* (a transcription factor with testis specific expression) was expressed
225 at much higher levels than controls (Figure 3A). Comparison to tissue-specific transcriptomes indicates
226 that the upregulated genes are usually expressed outside the larval nervous system from a broad range
227 of tissues, including a large cluster of genes that have testis-enriched expression, as well as ovary, fat
228 body, and digestive system (Figure 3D and Appendix Figure5A, B).

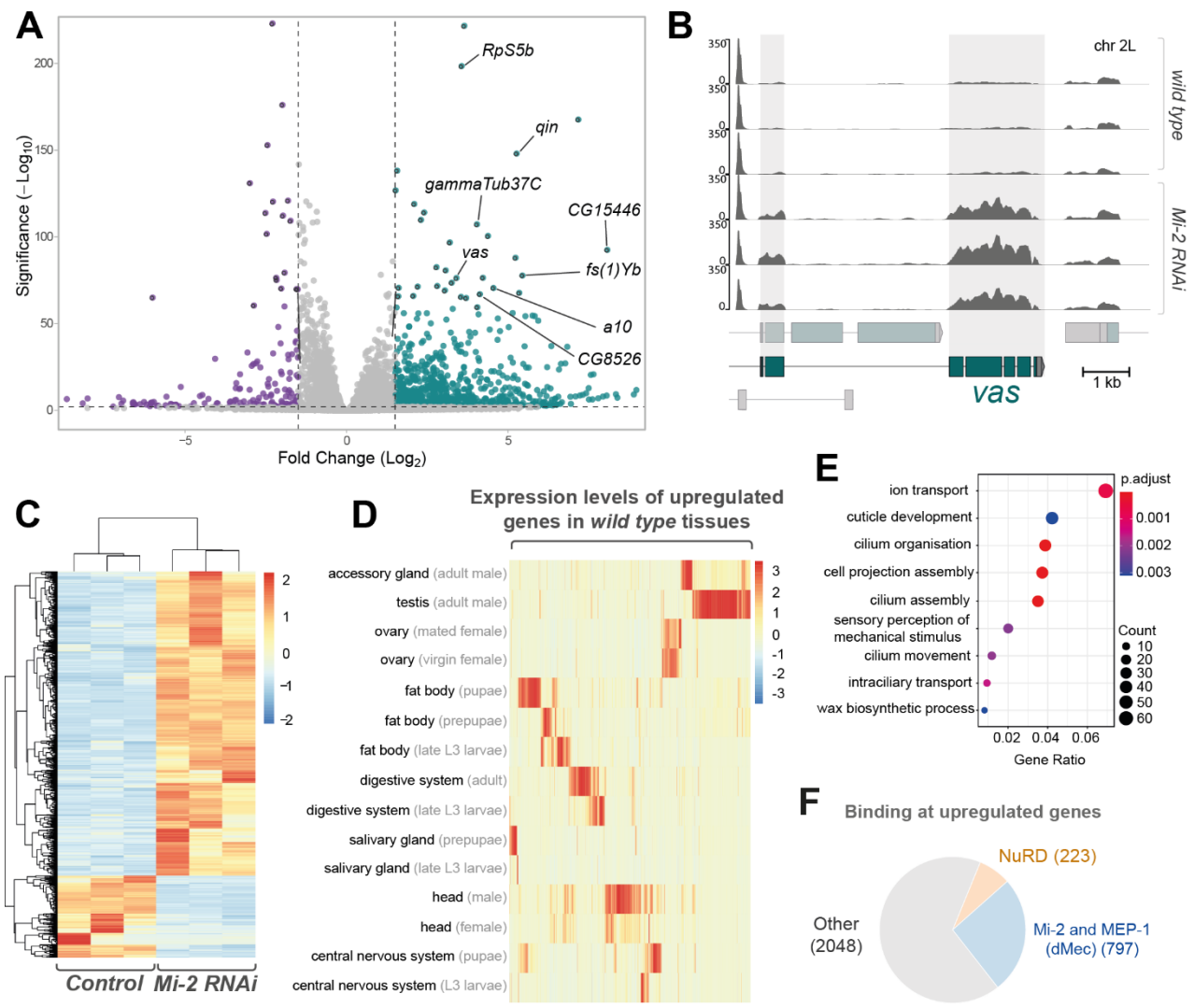

Figure 3. *Mi*-2 knockdown in larval neurons results in extensive gene expression changes. A) Volcano plot showing significantly up-regulated (green) and down-regulated (purple) genes with fold-change. Selected mis-expressed genes are annotated. B) RNA-seq tracks showing *vas* mRNA expression in third instar larval CNS (Y-axis is RPKM). C) Heatmap showing relative changes in normalised read-counts between *Mi-2* RNAi and control replicates for all significantly differentially expressed genes (p-adj < 0.05, log2 fold change >1 or <-1). Significantly more genes are upregulated (1467) than downregulated (397). D) Heatmap showing relative expression levels of upregulated genes across selected *Drosophila* tissues (full version in Appendix Figure 5A). E) Enriched gene ontology terms for genes that are upregulated in *Mi-2* RNAi knockdown. F) Proportion of differentially upregulated genes that directly intersect with Mi-2, MEP-1, MTA-1like and HDAC1 peaks, and differentially upregulated genes intersecting with exclusively Mi-2/MEP-1 or all NuRD subunits.

We also observed misexpression of neuronal lineage specific genes that are not usually highly expressed in the larval CNS but are expressed in specific neuronal populations in the adult nervous system. For example, the antennal gene *a10* was seen to be very highly upregulated upon knockdown of *Mi-2* in the larval CNS despite usually having expression restricted to the antennae in adult flies (Figure 3A and Figure EV1C). Therefore, these data indicate that Mi-2 is required to ensure fidelity of neuronal transcriptomes by suppressing expression of spatially and temporally inappropriate genes.

236 **Mi-2/dMEC represses ectopic gene expression independently of histone deacetylation**

237 Having seen that Mi-2/NuRD components are distributed unequally in the genome, we examined how
238 binding of NuRD components related to differentially upregulated genes. Since previous reports have
239 suggested that dMec has a role in suppressing ectopic gene expression in cultured cells, we questioned
240 whether this complex also plays a greater role in repressing ectopic gene expression in neurons. We
241 found that NuRD binding (i.e. significant binding of Mi-2, MTA1-like, and HDAC1) was found at a much
242 lower proportion of upregulated genes compared to those bound by dMec (Mi-2 and MEP-1) (223 and
243 797 genes respectively – (Figure 3F)). This observation led us to further investigate the role of dMec in
244 regulating gene expression compared to NuRD.

245 We used qPCR to confirm upregulation of a selection of highly mis-expressed candidate genes in *Mi-2*
246 knockdown flies (Figure 4A). Since RNAi mediated knockdowns have previously been associated with
247 off-target effects, we repeated these experiments with a second RNAi line which recapitulated the
248 upregulation of ectopic genes previously observed (Appendix figure 6). Since we saw distinct binding of
249 NuRD subunits, we first asked whether *HDAC1* was required for repression of ectopic genes. We found
250 that depletion of *HDAC1* by RNAi in neurons resulted in lethality during pupal stages similarly to *Mi-2*
251 (Appendix figure 7). However, *HDAC1* knockdown with two independent RNAi lines had no effect on
252 expression of any of the genes we tested that were upregulated upon *Mi-2* knockdown. Therefore, whilst
253 neuronal *HDAC1* is essential for survival, histone deacetylation is not required for repression of some
254 *Mi*-2 induced ectopic gene expression in larval neurons (Figure 4A and Appendix figure 6).

255 We questioned whether the expression of ectopic genes in *Mi-2* knockdown was dependent on NuRD
256 (albeit without HDAC1 activity) or mediated by Mi-2 via NuRD-independent mechanisms. To address
257 this, we knocked down *MBD-like,* a core NuRD component thought to bridge the nucleosome
258 remodelling and histone deacetylation subunits. In *MBD-like* RNAi knockdown neurons, no difference in
259 gene expression of ectopic target genes was observed (Figure 4A), providing further evidence of *Mi-2*
260 acting independently of NuRD to mediate gene repression. Since MEP-1 binding in the genome appeared
261 to coincide with Mi-2 at almost every locus, we hypothesised that MEP-1 must also be part of the same
262 complex that confers repression of ectopic gene expression. Consistent with this idea, we saw that
263 knockdown of MEP-1 with *elav*-GAL4 was sufficient to cause upregulation of *vas* along with other target
264 genes tested (Figure 4A). Therefore, it appears that dMEC represses the expression of some genes in a
265 MEP-1 and Mi-2 dependent manner, without the requirement for histone deacetylation or other
266 members of the NuRD complex.

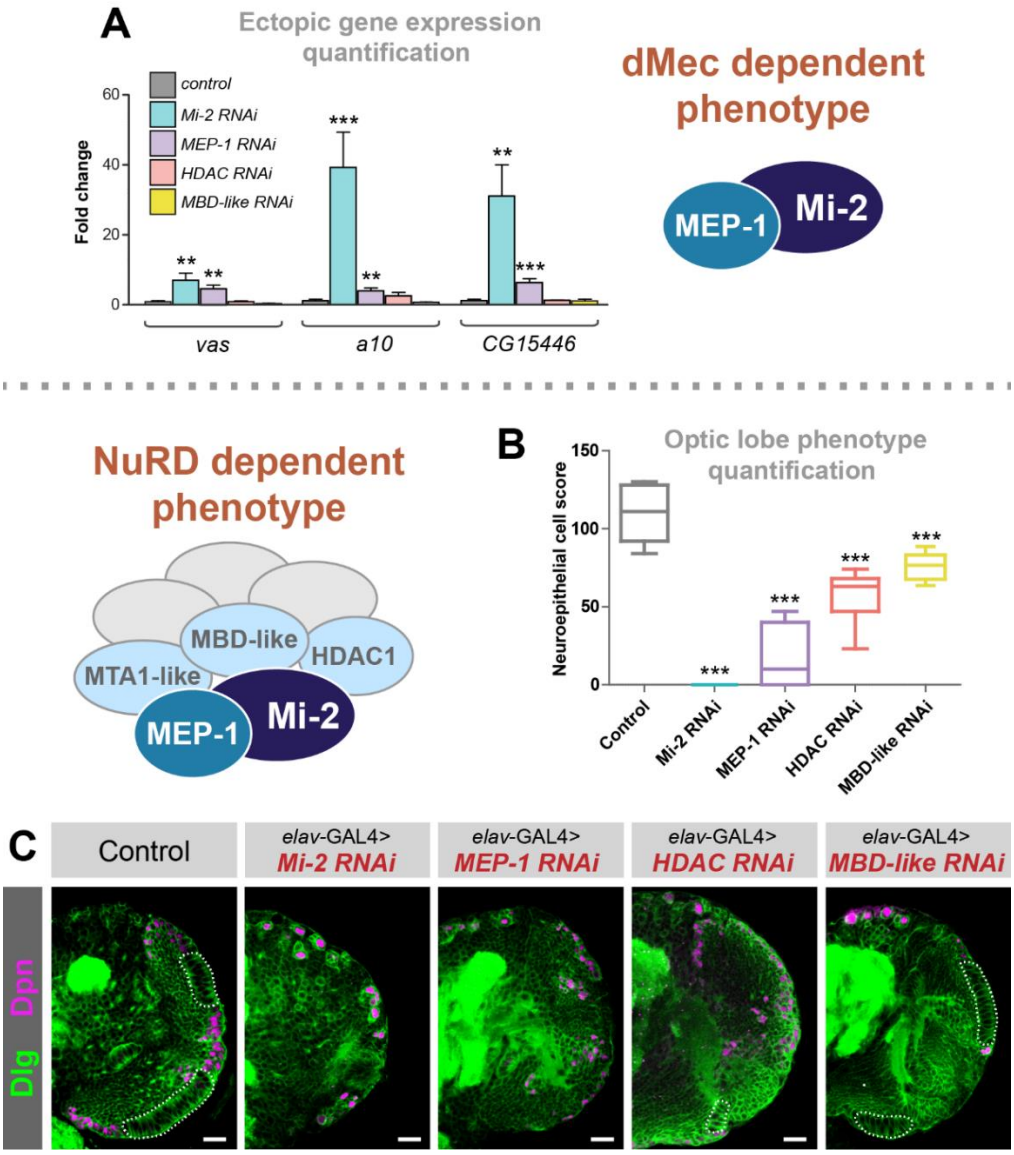

Figure 4. *dMec* knockdown causes ectopic gene expression and *NuRD* knockdown causes an optic lobe development phenotype.

A) Quantification of candidate gene expression (selected from upregulated genes in RNA-seq data) in knockdown genotypes (3 biological replicates for each group). ** $p < 0.01$ *and* *** $p < 0.001$ (one-tailed student's t-test or Welch's t-test against control) Represented as mean ± SEM. B) Quantification of optic lobe neuroepithelial cells of genotypes shown in panel C (n >= 9 for each group). *** $p < 0.001$ (one-tailed student's t-test or Welch's t-test against control). Represented as a box plot. C) Representative images of control (*elav*-GAL4*; ; mCherry*^{RNAi}), *Mi-2* knockdown, *MEP-1* knockdown, *HDAC1* knockdown and *MBD-like* knockdown in the third instar larval CNS (all scale bars = 20 µm). Discs large (Dlg) = green, Deadpan (Dpn) = magenta. Neuroepithelial cells are highlighted by dashed lines.

NuRD disruption in larval CNS causes severe optic lobe growth defects.

Performing GO analysis for down-regulated genes from our Mi-2 knockdown RNA-seq indicated enrichment of multiple terms related to cell division and stem cell function (Appendix figure 8). This is

surprising since we knocked down *Mi-2* in neurons, which are exclusively post-mitotic and do not express genes related to cell-division– therefore it is unlikely that Mi-2 could directly downregulate the expression of these genes. To further understand the consequences of *Mi-2* depletion in neurons, we examined dissected third instar larval CNS using confocal microscopy. We found that in *Mi-2* knockdown resulted in severe optic lobe defects. Mi-2 knockdown brains were smaller, and it was evident that all recognisable optic lobe structures (including inner and outer optic proliferation centres as well as differentiating medulla and lamina neurons) were found to be completely absent (Figure 4B,C). Interestingly, this included proliferative cells of the optic lobes and neuroepithelium (NE), including the neuroblasts. We also examined *Mi-2* knockdown ventral nerve cords (VNCs) and observed no morphological changes or differences in NSC numbers (Appendix Figure 9). Therefore, we attributed the enrichment of GO terms relating to precursor cell function to the fact that a large number of cells expressing these genes were not present in the tissue from which RNA was extracted. Due to this severe phenotype, in which a large fraction of optic lobe cells are absent, we decided that we could not reliably identify genes that were downregulated as a consequence of Mi-2 loss rather than due to absence of cells expressing those genes. However, since we still saw far fewer downregulated than upregulated genes, this reinforces our conclusion that Mi-2 mainly acts to suppress gene expression in this context.

Having seen NuRD-independent effects of *Mi-2* on gene expression, we questioned whether knockdown of other NuRD complex components would phenocopy the optic lobe phenotype we observed when *Mi-2 was* knocked down with *elav*-GAL4. In *MEP-1*, *HDAC1* and *MBD-like* knockdowns, the larval CNS displayed a similar optic lobe defect to that of *Mi-2* (Figure 3A). Quantification of NE cells indicated that *MEP-1*, *HDAC1* and *MBD-like* knockdowns had significantly fewer NE cells (Figure 3B), however the phenotype was less severe with a small number being present in most brains (although this may be due to less efficient RNAi mediated knockdowns in these lines). (Burgold et al., 2019) We also observed an optic lobe phenotype with knockdown of *MTA-1* (Appendix Figure 10). Therefore, due to the similarity of phenotypes observed with knockdowns of multiple NuRD complex members we concluded that whilst *Mi-2* functions to repress some ectopic genes in a NuRD independent manner, its effect on optic lobe development involves the activity of the NuRD holocomplex. Conversely, the ectopic upregulation of genes is independent of NuRD/histone deacetylation, and is not required to produce optic lobe developmental defects in the larva (although since the phenotypes vary in severity, there may be some contribution of dMec induced ectopic gene expression on NE survival).

Fully differentiated neurons do not require Mi-2 for silencing of ectopic gene expression or proper optic lobe development

Factors involved in the maintenance of neuronal transcriptomes during early neuronal maturation can have less severe phenotypes in fully differentiated neurons in which synapses have been formed (Hassan et al., 2020; Southall et al., 2014). This correlates with observed changes to the underlying chromatin landscape which is dynamic during differentiation and neuronal maturation (Aughey et al.,

308 2018; Marshall and Brand, 2017). Notch-induced hyperplasia in neuronal lineages is enhanced by the
309 knockdown of *Mi-2*, however, this effect is diminished as cells become more differentiated
310 (Zacharioudaki et al., 2019). In our previous knockdown experiments, we employed the *elav*-GAL4
311 driver to target all neurons in the *Drosophila* larval CNS. This includes a substantial proportion of
312 neurons that are post-mitotic cells, but not fully differentiated to the point at which synaptic proteins
313 are expressed. In fact, it has been suggested that the majority of larval brain *elav*-expressing neurons
314 contribute relatively little to neuronal function (Eichler et al., 2017), since they do not possess axons or
315 dendrites or express ion-channels associated with neurotransmission (Ravenscroft et al., 2020), despite
316 comprising a large proportion of the total cells in the larval brain (Jiao et al., 2021). Therefore, we
317 questioned whether Mi-2 dependent optic lobe phenotypes or de-repression of silenced genes would be
318 observed when Mi-2 was knocked down in either progenitor cells or fully differentiated neurons.

319 We used *wor*-GAL4, to drive *Mi-2* RNAi in NSCs. Surprisingly, we found that *Mi-2* knockdown in NSCs
320 showed no apparent defects in optic lobe development, with brain lobes having a similar morphology
321 and neuroepithelial cell numbers to controls (Figure 5B and Figure EV2A). In contrast to when *Mi-2* was
322 depleted in neurons (Figure 1D), loss of *Mi-2* in NSCs did not result in larval locomotion defects
323 (Appendix figure 11). However, *Mi-2* knockdown in NSCs did result in lethality, with 100% dying as
324 pupae. Therefore, since brain size, morphology and movement are normal in these animals, these results
325 suggest that Mi-2 is not required for stem cell division or differentiation into neurons. Nevertheless, Mi-
326 2 function in NSCs is required for the correct functioning of subsequently born neurons.

327 *elav*-GAL4 may drive some expression in embryonic glial cells (Berger et al., 2007), therefore, we
328 questioned whether unexpected glial knockdown of *Mi-2* may have resulted in a disruption of signalling
329 that maintains the optic lobe stem cells. To address this, we repeated the *Mi-2* knockdown with an *elav*-
330 GAL4 driver combined with *repo*-GAL80, to repress unwanted expression of the RNAi hairpin in glia. In
331 these animals, we observed the same severe optic lobe phenotype as previously with *elav*-GAL4 alone
332 (Appendix Figure 13). These data indicate that *Mi-2* knockdown in neurons may affect optic lobe growth
333 via a non-cell-autonomous mechanism. This may be partly explained by the requirement for innervation
334 by photoreceptor neurons to initiate neurogenesis in the developing visual centres (Huang and Kunes,
335 1996; Selleck and Steller, 1991), which would be affected by *elav*-GAL4 knockdown of *Mi-2*. We also
336 examined 1st instar *Mi-2* knockdown brains and found that the typical rosette of NE cells is present
337 (Appendix Figure 14). Therefore, the NE is present at earlier stages of development, however, is not
338 perduring to later stages. As *elav*-GAL4 has never been reported to be expressed in NEs, the role of any
339 glial expression of *Mi-2* RNAi has been eliminated (Appendix Figure 13), and knockdown of *Mi-2* in
340 neuroblasts has no phenotype (Figure EV2A), this strongly suggests that there is a non-cell-autonomous
341 mechanism occurring. However, a full explanation of this phenotype is beyond the scope of this study
342 and further work must be conducted to determine the mechanism by which the optic lobe defect occurs.

343

344 Since we observed differences in the severity of observed phenotypes resulting from *Mi-2 knockdown* in
345 neurons or NSCs, we questioned whether Mi-2 was required for suppression of ectopic gene expression
346 in NSCs or precursor cells. Using *wor*-GAL4 to knock down *Mi-2* in NSCs, we performed qPCR to detect
347 changes in gene expression. When *Mi-2* was knocked down in NSCs, the expression of female germline
348 marker *vas* was significantly upregulated (Figure 5C), as previously seen with *elav*-GAL4 knockdowns.
349 *vas* expression was upregulated to a lower extent than when induced with *elav*-GAL4 (~4 fold increase
350 compared to ~10 fold), however this may be due to the lower number of affected cells expressing *wor*-
351 GAL4 rather than reflecting a difference in the requirement for Mi-2 for repression of *vas* in NSCs. It
352 should also be noted that it is possible that a small amount of perdurance of GAL4 into NSC progeny may
353 be responsible for de-repression of non-neuronal target genes in immature neurons or GMCs, rather
354 than due to an effect exclusively in NSCs.

355 Next, we examined brains in which *Mi-2* RNAi was driven with *nSyb*-GAL4 which is exclusively expressed
356 in more mature synapse forming neurons. In contrast to knockdown in all neurons including immature
357 neurons with *elav*-GAL4, depletion of *Mi-2* exclusively in mature neurons did not produce overt
358 morphological phenotypes and no significant difference in neuroepithelial cell numbers were detected
359 when compared to controls (Figure 5B and Figure EV3B). As with the other drivers used, *Mi-2*
360 knockdown with *nSyb*-GAL4 resulted in 100 % lethality during pupal stages. Therefore, whilst Mi-2 is
361 required in mature neurons, the morphological defects observed do not arise from loss of Mi- 2 function
362 in fully differentiated neurons in the larval CNS.

363 Knockdown of *Mi-2* using *nSyb*-GAL4 did also not result in any detectable change in *vas* mRNA levels
364 (Figure 5C). We also tested whether depletion of *Mi-2* in adult neurons was sufficient to de-repress *vas*
365 expression using a temperature sensitive GAL80 to de-repress *Mi-2* RNAi in neurons using *elav-GAL4*
366 for a 24-hour period after eclosing. As in third instar larvae, no change in *vas,* expression was detectable
367 in adult heads (Appendix Figure 12). We also tested for expression of *a10* and *CG15446*, which also did
368 not show any increased expression in adult neurons, indicating that Mi-2 is only required for the
369 repression of ectopic gene expression in the early stages of neuronal development.

370 **Dynamic Mi-2 binding during neuronal differentiation**

371 We reasoned that varying consequences of *Mi-2 loss* at different stages of neuronal differentiation may
372 be reflected by changes to Mi-2 binding in different cell types. To examine how Mi-2 genome occupancy
373 changes as neurons are born and mature, we profiled Mi-2 (using TaDa) in NSCs (*wor*-GAL4) and mature
374 neurons (*nSyb*-GAL4) in the larval CNS.

375 Binding profiles between cell types were compared and regions of differential binding identified (Figure
376 5 D,F). Total neurons (*elav*-GAL4) show the largest number of significantly bound peak regions (10,420),
377 with mature neurons binding 7054 genes (Figure 5E). However, the number of peaks common to each
378 cell type is relatively low. Therefore, Mi-2 binding is highly dynamic during neuronal differentiation.

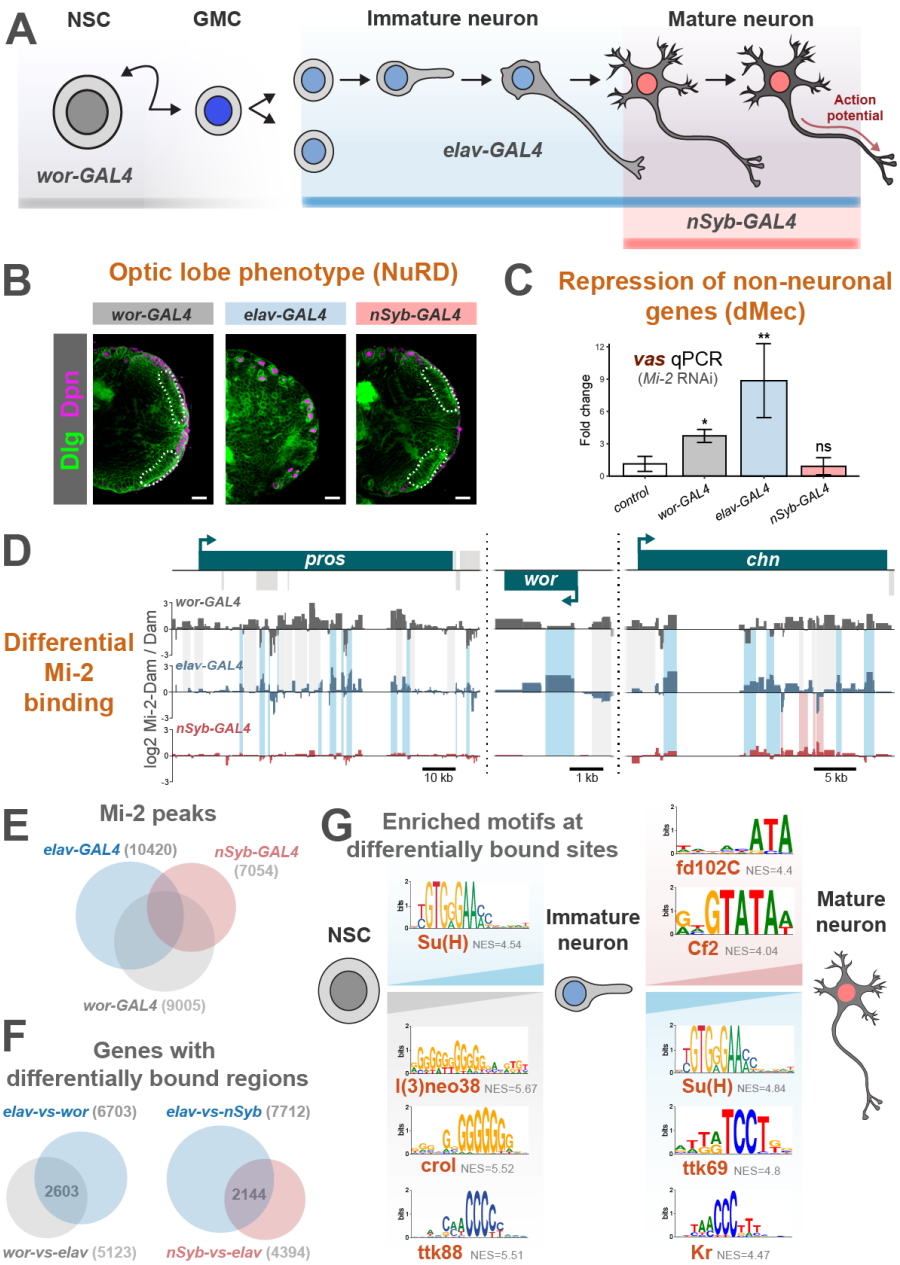

Figure 5. Differential requirements and binding of Mi-2 during neuronal differentiation. A) Representation of expression of GAL4 drivers used. B) Larval brain optic lobe morphology when *Mi-2* is knocked down at different stages of differentiation Elav = green, Dpn = magenta. C) Ectopic expression of *vas* when *Mi-2* is knocked down at different stages of differentiation. (3 biological replicates for each group). * $p < 0.05$ and ** $p < 0.01$ (one-tailed student's t-test against control) Represented as mean ± SEM. D) Examples of differential genomic binding of Mi-2 at neural genes. E) Overlap of Mi-2 binding peaks in NSCs, immature neurons and mature neurons. F) Number and overlap of genes with differential Mi-2 binding. G) Motif analysis of differentially bound regions.

In many individual genes, sites with enriched binding in NSCs showed a different set of enriched Mi-2 binding sites in immature neurons (Figure 5 D, F). A similar change occurs from immature to mature neurons, with 2144 genes that contain both immature-vs-mature and mature-vs-immature regions of Mi-2 enrichment (Figure 5E and the example of *chn* in Figure 5C).

Motif enrichment analysis of the differentially bound regions identified transcription factor binding sites (Figure 5G). Binding sites for l(3)neo38, crol and ttk88 are present in the NSC-vs- immature comparison,

386 suggesting that these sites are occluded in NSCs but available for binding in neural progeny.
387 Interestingly, l(3)neo38 occupies a set of putative neuronal enhancers in the developing embryo and is
388 required for the proper formation of the larval brain (Reddington et al., 2020). l(3)neo38 and crol have
389 both been implicated in the regulation of heterochromatin silencing (Schneiderman, 2010 & Swenson,
390 2016). While ttk88 sites are enriched for binding in NSC-vs-immature neurons, ttk69 sites (a different
391 splice isoform) are enriched in the immature-vs- mature comparison. Finally, fd102C and Cf2 sites have
392 greater Mi-2 binding in mature-vs-immature neurons. Fd102C is an uncharacterised forkhead
393 transcription factor highly expressed in the developing and adult nervous system (Krause et al., 2022)
394 and Cf2 is a zinc-finger factor involved in follicle cell fate and myogenic gene expression (Bagni et al.,
395 2002; Hsu et al., 1996). These data indicate that a dynamic repertoire of transcription factors may direct
396 or be influenced by dynamic Mi-2/NuRD binding during neuronal maturation. It is clear from the broad
397 changes in binding that Mi-2 coordinates a distinct gene expression programme in early neuronal
398 lineages compared to fully differentiated neurons corresponding to the differences in phenotypic
399 outcomes observed.

400 Su(H) (Notch co-factor) motifs were enriched in both immature-vs-NSC and immature-vs-mature
401 regions (Figure 5G). This aligns with previous work showing that Mi-2 is required to deactivate notch
402 responsive stem-cell enhancers in neuronal progeny (Zacharioudaki et al., 2019). Mi-2 was implicated
403 in the silencing of genes in the *E(spl)-C* locus, with broad binding of Mi-2 across this locus having been
404 demonstrated in *Drosophila* cell lines (Ho et al., 2014; Kreher et al., 2017). Consistent with this result we
405 saw strong binding of Mi-2 across the *E(spl)-C* locus in both NSCs and immature neurons (Figure EV3).
406 This study also showed that in more mature neurons Mi-2 depletion was not sufficient to enhance notch-
407 induced overgrowth. We saw no significant binding of Mi-2 in mature neurons across the entire region
408 (approx. 50 kb), supporting the conjecture that in more fully differentiated cells, continued chromatin
409 remodelling of the *E(spl)* genes by Mi-2 is not required for their repression.

410

411 **Discussion**

412 Our data provide evidence for Mi-2 activity in repressing ectopic gene expression independently of
413 NuRD. Mi-2 from *Drosophila* or humans is sufficient for the remodelling of nucleosomes *in vitro*, in the
414 absence of other NuRD components (Brehm et al., 2000; Wang and Zhang, 2001). In mouse embryos,
415 Mi-2 orthologue CHD4 was shown to be necessary for lineage specification in a manner that was
416 independent of MBD proteins that are required for a functional NuRD complex (O'Shaughnessy-Kirwan
417 et al., 2015). Similarly, loss of CHD4 in human erythroid cells resulted in de-repression of fetal *γ-globin*,
418 which occurred independently of NuRD (Amaya et al., 2013). Furthermore, similarly to what we observe
419 in neurons, MBD3 was found to bind at less than half of all CHD4 sites in mouse ESCs and were anti-
420 correlated to histone markers associated with transcription (Bornelov et al., 2018). Therefore, it is likely
421 that NuRD-independent Mi-2 regulation of gene expression is a conserved feature in animal cells.

422 A previous study concluded that Mi-2 in complex with MEP-1 (dMec) was the dominant Mi-2 containing
423 complex in *Drosophila* Kc cells (Kunert et al., 2009). From this observation it could be inferred that NuRD
424 plays a relatively minor role in the regulation of gene expression. However, this conclusion was drawn
425 based on biochemical interactions and relative stoichiometries of NuRD components. We find that in
426 contrast to the abundance of dMec, around a third of Mi-2 peaks intersect with MTA1-like, indicating
427 that NuRD is prevalent at a large number of loci. Furthermore, severe optic lobe phenotypes were
428 observed with multiple NuRD components, which did not always include de-repression of lineage-
429 inappropriate genes. These data indicate that despite being present at lower amounts than dMec, NuRD
430 plays a critical role in nervous system development. Whilst it is possible that the proportions of
431 NuRD/dMec may differ between the CNS and cultured cells, our data suggest that the relative amounts
432 of protein detected by biochemical means may not be reflective of either the distribution of sites at
433 which complexes are associated in the genome, or the severity of consequences resulting from their loss.
434 There is currently unclear whether an analogous complex to dMEC exists in mammals. MEP-1 does not
435 share direct orthology with any single mammalian transcription factors, however, since it is clear that
436 CHD4 is capable of conferring NuRD-independent activities in mammalian cells, it is possible that there
437 are unidentified mammalian genes that act in an analogous role to MEP-1.

438 Our data indicates that Mi-2 represses non-neuronal genes such as those normally expressed in the
439 germline, and that this is largely independent of NuRD. Interestingly, Mi-2/dMec depletion resulted in
440 proneural gene expression in Kc cells (Kunert et al., 2009), suggesting that Mi-2 may repress ectopic
441 gene expression in multiple tissue types dependent on context. A similar phenotype has also been
442 reported in *C. elegans* in which MEP-1/Mi-2 knockdown resulted in expression of germline genes in
443 somatic tissues, indicating that this may be a conserved function of Mi-2 (Unhavaithaya et al., 2002). It
444 is possible that in mammals, NuRD-independent CHD4 function is also required for gene repression
445 since loss of CHD4 in lymphocytes results in upregulation of non-hematopoietic genes (Arends et al.,
446 2019). However, it remains unclear whether this transcriptional repression is dependent on histone
447 deacetylase activity/NuRD, or NuRD-independent CHD4 activity.

448 Mi-2 is only required to suppress ectopic gene expression up to the early stages of neuronal
449 development, whereas in more fully differentiated cells it is dispensable . Therefore, it is likely that other
450 molecular factors are required for the repression of these genes following synaptogenesis. Mi-2/dMEC
451 may be required to establish a stable epigenetic state following recruitment by sequence specific
452 transcription factor binding, after which these states are maintained by separate chromatin modifying
453 proteins or complexes. The degree of differential binding of Mi-2 observed during neuronal
454 differentiation is consistent with the idea that Mi-2 coordinates a distinct gene expression programme
455 during early neuronal differentiation compared to in mature neurons. The identification of different
456 transcription factor binding sites during development suggests that either the cognate transcription
457 factor is recruiting Mi-2 to these sites, or that Mi-2 is independently positioned there to establish a
458 chromatin state to prevent the binding of the factor. Since it seems that Mi-2 exhibits at least two

459 independent modes of interacting with chromatin (i.e. via dMEC/NuRD), either or both of these models
460 may be true depending on the presence of other subunits and wider genomic context. Su(H) binding
461 sites are found at sites enriched in immature neurons versus both NSCs and mature neurons (Figure
462 5G). Furthermore, l(3)neo38 binding sites, that have been identified at neural enhancers (Reddington
463 et al., 2020), are more strongly bound in NSCs compared to immature neurons. Therefore, for at least
464 Su(H) and l(3)neo38, Mi-2 appears to be blocking binding of these factors (loci specific) at stages of
465 differentiation where their function is not required/wanted.

466 Together, our data highlight that the activity of Mi-2 is dependent on both its molecular and
467 developmental context. These data highlight the importance of detailed analyses of individual subunits
468 in inferring functions of chromatin modifying complexes in complex multicellular tissues to fully
469 understand their role in gene regulation.

470

471 # Materials and Methods

472 **Fly stocks**

473 Unless stated otherwise flies were kept on standard fly food media at 25 degrees. A full list of fly stocks
474 used in this study can be found in Appendix Table S1. Mixed sex larvae/flies were used for all
475 experiments.

476 **Immunohistochemistry and imaging**

477 Third instar larval CNS were dissected in PBS and fixed for 20 min with 4% formaldehyde in PBS. The
478 following antibodies were used in this study: rat anti-Elav (7E8A10 - Developmental Studies Hybridoma
479 Bank), chicken anti-GFP (600-901-215 - Thermo scientific), mouse anti-DLG (4F3 - Developmental
480 Studies Hybridoma Bank), and guinea pig anti-Dpn (kind gift from A. Brand). Samples were imaged using
481 a Zeiss LSM510 confocal microscope and images processed using LSM Image Browser and image J. To
482 quantify an OPC NE cell score for each genotype, 3rd instar larval brains were mounted dorsal side down
483 and full image stacks (2 µm intervals) of the brain lobe were taken using the DLG channel. The number
484 of OPC NE cells were counted at image slices at ¼, ½ and ¾ through the stack (identified by position
485 and morphology) and added together to give the score. To quantify the number of Dpn positive cells in
486 VNCs, , whole VNC image stacks were analysed using the 3D Objects Counter in Fiji (Bolte and
487 Cordelieres, 2006). For each genotype, a Shapiro–Wilks test was performed to calculate if the
488 experimental and control data had normal distributions. If they did, a one-tailed student's t-test was
489 applied, and if not a Welch's t-test was applied.

490 **Generation of Targeted DamID lines**

491 *MEP-1* and *Mi-2* were amplified by PCR from cDNA with primers including 30 bp complementary
492 sequence to *pUASTattB-LT3-Dam* (Southall et al., 2013) (see Appendix Table S2). Linearised *pUAST-LT3-*
493 *Dam* (digested with NotI and XbaI) was combined with either *MEP-1* or *Mi-2* PCR-amplified coding
494 sequences in a Gibson assembly reaction using NEBuilder® HiFi DNA Assembly kit (NEB) following
495 manufacturers protocols. Resulting N-terminal fusion constructs were injected into *attP2* flies (*y w*
496 *P{y[+t7.7]=nos-phiC31\int.NLS}X #12;; P{y[+t7.7]=CaryP}attP2* – Department of Genetics Microinjection
497 Service, Cambridge) for integration on the third chromosome.

498 *UAS-MTA-1-like-Dam* and *UAS-HDAC1-Dam* were generated using the FlyORF-TaDa cassette exchange
499 protocol as previously described (Aughey et al., 2021). Briefly, *UAS-HDAC1* and *UAS-MTA1-like* FlyORF
500 lines were crossed to *hsFLP; TaDa-FlyORF.* Progeny were heat-shocked at 37 degrees for 45 mins at 96
501 hours following larval hatching. Resulting males were crossed to *Dr/TM6B* and white-eyed F2 males and
502 female virgins used to create a stable stock.

503 **Targeted DamID**

504 Dam fusion or Dam-only males were crossed to virgins of the appropriate driver line for expression of
505 Dam in the desired cell-types. For expression in NBs, all larval neurons (including immature neurons),
506 or mature neurons only - the drivers *wor*-GAL4*; tub*-GAL80^{ts}*, elav*-GAL4*; tub*-GAL80^{ts}*, and nSyb*-GAL4*;*
507 *tub*-GAL80^{ts}*,* were used, respectively. Embryos were collected for 4 hr then raised at 18°C to prevent
508 premature Dam expression. Animals were transferred to 29°C at 8 days after embryo deposition for 24
509 hours. 60 larval central nervous systems were dissected and stored at -80 degrees. Genomic DNA
510 extraction, methylated DNA enrichment and library preparation were carried out as previously
511 described (Marshall et al., 2016). Two biological replicates were generated for each experiment.

512 Libraries were sequenced with 50 bp single end sequencing on Illumina HiSeq or NovaSeq platforms.
513 >15 million reads were obtained for each library. Data were processed using a previously described Perl
514 pipeline (Marshall and Brand, 2015) (https://github.com/owenjm/damidseq_pipeline).

515 Peak calling was performed using a previously described Perl program (available at
516 https://github.com/tonysouthall/Peak_calling_DamID) which allows for the identification of broadly
517 bound regions that characterise DamID data (Estacio-Gomez et al., 2020). Briefly, false discovery rate
518 (FDR) was calculated for regions consisting of >1 GATC bounded fragments for each replicate.
519 Significant (FDR<0.01%) regions present in all replicates are merged to form a final peak file. Enriched
520 motifs discovery was performed using i-cisTarget on significant peak regions (Herrmann et al., 2012).
521 Intersecting regions for comparison of binding between Mi-2, MEP-1, MTA1-like, or HDAC1 were
522 computed using bedtools intersect utility (Quinlan and Hall, 2010). Similarity between binding peaks
523 was determined using the bedtools jaccard utility, which calculates the ratio between the number of
524 intersecting base pairs and the union between two coordinate sets (Favorov et al., 2012).

525 **Larval crawling assays**

526 Larval crawling assays were conducted as in (Nichols et al., 2012). Briefly, individual third instar
527 wandering larva were placed on room temperature agar with a 10 mm^2 grid placed underneath as a
528 distance reference. Larvae were left to acclimatise for 1 min after which larval movement was tracked
529 visually. Ten animals were used per genotype with three technical replicates performed per animal.

530 **Developmental survival assays**

531 Flies of the appropriate genotype were left in cages containing standard food media supplemented with
532 yeast and left to acclimatise over three nights at 25 °C. Food media was exchanged for apple juice agar
533 and flies left to lay for 5 h. Following the laying period, 100 embryos were transferred to fresh food vials
534 to allow for counting of surviving adults and pupae.

535 **RNA extraction**

536 Three biological replicates were used for knockdown or control samples. Third instar larval CNS were
537 dissected from thirty animals per replicate and total RNA extracted using TRIzol reagent
538 (https://tools.thermofisher.com/content/sfs/manuals/trizol_reagent.pdf) following suppliers
539 protocols. Library preparation and sequencing were subsequently performed by Beijing Genomics
540 Institute (BGI). Sequencing data was mapped to the *Drosophila* genome (release 6.22) using STAR
541 (Dobin et al., 2013). Mapped files were collected in a matrix using featureCounts from the Rsubread
542 package (Liao et al., 2019). Differential expression analysis and MA plots were carried out using the
543 Deseq2 R package (Love et al., 2014).. Genes that had an adjusted p-value <0.05 and a log2 fold change
544 greater than 1 (for upregulated) or less than -1 (for downregulated) were classified as significant.
545 Heatmap generated using pheatmap package in R. Analysis of tissue specific gene enrichment was
546 performed using DGET (Hu et al., 2017).

547 **qRT-PCR**

548 Following RNA extraction, reverse transcription was performed using the iScript cDNA synthesis kit
549 (Bio-Rad), following manufacturer's protocols. qRT-PCR was carried out using iTaq Universal SYBR
550 Green Supermix (Bio-Rad). Expression of target genes was normalised to *Ribosomal Protein L4* (*Rpl4*)
551 and compared to expression in control samples expressing RNAi targeting *mCherry*. Primers amplifying
552 sequences <200 bp were designed to span exon junctions where possible (sequences used can be found
553 in Appendix Table S2. Three biological replicates were carried out for each genotype, with at least two
554 technical replicates for each biological replicate. For each genotype, a Shapiro–Wilks test was performed
555 to calculate if the experimental and control data had normal distributions. If they did, a one-tailed
556 student's t-test was applied, and if not a Welch's t-test was applied.

557

558 **Data availability**

559 All raw sequence files and processed files have been deposited in the National Center for Biotechnology
560 Information Gene Expression Omnibus (GSE199146).

561 **Acknowledgments**

562 We would like to thank the Southall lab and Imperial College fly community for help and feedback on
563 this project. We would like to thank Andrea Brand for generously providing fly stocks and the Dpn
564 antibody. We also thank the Bloomington *Drosophila* Stock Center (NIH P40OD018537) for fly stocks.
565 This work was funded by a Wellcome Trust Investigator grant 104567 to T.D.S and a BBSRC grant
566 BB/P017924/1 to T.D.S. and G.N.A.

567 **Disclosure and competing interests statement**

568 The authors have no conflicts of interest to disclose.

569 **Author contributions**

570 GNA, EF, KG, SZ and TDS performed experiments. GNA and TDS performed analyses, wrote the
571 manuscript and designed experiments.

572

573 # Figure Legends

574 **Figure 1. Critical role of *Mi-2* RNAi in *Drosophila* neurons.** A) Third instar larval CNS of *Mi-2* GFP-
575 trap line (scale bar = 20 μm). White arrows highlight NSC nuclei. B) Survival of *Mi-2* RNAi and control
576 (*mCherry-RNAi*) flies during development (**** p < 0.001).* D) Larval crawl speed (cm/minute) in *Mi-2*
577 RNAi and *mCherry* RNAi controls (** *p < 0.01*).

578 **Figure 2. Figure 2. Genomic binding of NuRD components.** A) Principal component analysis of all
579 NuRD component binding in neurons including replicates. Mi-2/MEP-1 (blue/purple) cluster
580 independently of MTA1-like (green) and HDAC1 (orange) reflecting greater similarity in their binding
581 profiles. B) Heatmap and enrichment plots indicating binding at Mi-2 peaks. C) Top enriched motifs at
582 NuRD and dMec peaks. D) Venn diagrams indicating the number of overlapping peaks between NuRD
583 subunits. All intersections between peaks occur at statistically significant frequencies (Fisher's exact
584 test $p < 10^{-24}$). E) Peak annotation for Mi-2, MEP-1, MTA-1like and HDAC1 peaks. F) Proportion of
585 differentially upregulated genes that directly intersect with Mi-2, MEP-1, MTA-1like and HDAC1 peaks,
586 and differentially upregulated genes intersecting with exclusively Mi-2/MEP-1 or all NuRD subunits.
587 G) Heatmap indicating jaccard similarity statistic between chromatin states and NuRD peaks (Mi-2,
588 MEP-1, MTA-1like and HDAC1) and dMEC (Mi-2 and MEP-1 only), or HDAC1 peaks.

589 **Figure 3. *Mi-2* knockdown in larval neurons results in extensive gene expression changes.** A)
590 Volcano plot showing significantly up-regulated (green) and down-regulated (purple) genes with fold-
591 change. Selected mis-expressed genes are annotated. B) RNA-seq tracks showing *vas* mRNA expression

592 in third instar larval CNS (Y-axis is RPKM). C) Heatmap showing relative changes in normalised read-
593 counts between *Mi-2* RNAi and control replicates for all significantly differentially expressed genes (p-
594 adj < 0.05, log2 fold change >1 or <-1). Significantly more genes are upregulated (1467) than
595 downregulated (397). D) Enriched gene ontology terms for genes that are upregulated in *Mi-2* RNAi
596 knockdown. E) Heatmap showing relative expression levels of upregulated genes across selected
597 *Drosophila* tissues (full version in Appendix Figure 5A).

598 **Figure 4. *dMec* knockdown causes ectopic gene expression and *NuRD* knockdown in neurons**
599 **causes an optic lobe development phenotype.**
600 A) Quantification of candidate gene expression (selected from upregulated genes in RNA-seq data) in
601 knockdown genotypes (3 biological replicates for each group). ** *p < 0.01 and *** p < 0.001* (one-tailed
602 student's t-test or Welch's t-test against control) Represented as mean ± SEM. B) Quantification of
603 optic lobe neuroepithelial cells of genotypes shown in panel C (n >= 9 for each group). *** *p < 0.001*
604 (one-tailed student's t-test or Welch's t-test against control). Represented as a box plot. C)
605 Representative images of control (*elav*-GAL4*; ; mCherry*^{RNAi}), *Mi-2* knockdown, *MEP-1* knockdown,
606 *HDAC1* knockdown and *MBD-like* knockdown in the third instar larval CNS (all scale bars = 20 µm).
607 Discs large (Dlg) = green, Deadpan (Dpn) = magenta. Neuroepithelial cells are highlighted by dashed
608 lines.
609

610 **Figure 5. Differential requirements and binding of Mi-2 during neuronal differentiation.** A)
611 Representation of expression of GAL4 drivers used. B) Larval brain optic lobe morphology when *Mi-2*
612 is knocked down at different stages of differentiation Elav = green, Dpn = magenta. C) Ectopic
613 expression of *vas* when *Mi-2* is knocked down at different stages of differentiation. (3 biological
614 replicates for each group). * *p < 0.05* and ** *p < 0.01* (one-tailed student's t-test against control)
615 Represented as mean ± SEM. D) Examples of differential genomic binding of Mi-2 at neural genes. E)
616 Overlap of Mi-2 binding peaks in NSCs, immature neurons and mature neurons. F) Number and
617 overlap of genes with differential Mi-2 binding. G) Motif analysis of differentially bound regions.

618 Expanded View Legends

619 **Figure EV1. Differentially expressed genes.** A) Read coverage for A) *gammaTub37C* and B) *RpS5b* loci,
620 which are non-CNS genes ectopically expressed in *Mi-2* knockdown. C) Heatmap showing relative
621 changes in normalised gene expression for the thirty most significantly up-regulated genes. D) Heatmap
622 showing relative changes in normalised gene expression for the thirty most significantly down-
623 regulated genes.

624 **Figure EV2. Quantification of neuroepthelial cells in NSC and mature neuron *Mi-2* knockdown**
625 **brains.** A) Representative images of optic lobes for control and *Mi-2* knockdown in NSCs. B)
626 Representative images of optic lobes for control and *Mi-2* knockdown in mature neurons. C) and D)
627 Quantification of optic lobe neuroepithelial cells of genotypes shown in panels A and B (n >= 7 for each

group). No significant difference found. Represented as a box plot. No significant difference found (one-tailed student's t-test).

Figure EV3. Mi-2 binding at the *E(spl)* complex is lost in mature neurons. Grey boxes represent genes.

Appendix Figure Legends

Appendix figure S1. Quality control for Targeted DamID data. Correlation between NuRD subunits (including replicates) in larval neurons (*elav*-GAL4). Very strong correlations are seen between Mi-2 and MEP-1 binding while the correlation between Mi-2/MEP-1 and either MTA-1like or HDAC1 are relatively lower. Good correlations are exhibited between replicates for each subunit (spearman's correlation r^2=0.85-0.95).

Appendix figure S2. GO analysis of NuRD and dMec gene targets. A) GO analysis of NuRD gene targets. B) GO analysis of dMec gene targets genes.

Appendix figure S3. Metagene analysis of HDAC1 binding. TSS is Transcriptional Start Site and TES is Transcriptional End Site.

Appendix figure S4. RNA-seq quality control. A) Heatmap and B) scatter plot showing Pearson correlation of RNA-seq reads between biological replicates and control and experimental groups. Very strong correlations are observed between replicates (R^2 > 0.97) with slightly lower correlations between knockdown and controls reflecting the changes in *Mi-2* RNAi transcriptome. C) Genome browser tracks indicating RNA-seq read coverage at the *Mi-2* locus. *Mi-2* reads are clearly depleted in *Mi-2 RNAi* compared to *elav*-GAL4 *x mCherry RNAi* controls (adjusted p value < 2.2×10^{-227}).

Appendix figure S5. Expression of differentially expressed genes in other tissues. A) Heatmap showing relative expression levels of upregulated genes across all tissues. B) Stacked bar plot showing percentage of upregulated genes that are expressed at different levels in specific tissues. Note that many upregulated genes are expressed at "very low" levels in the fly CNS, whilst upregulated genes are frequently expressed at "moderate" to very high levels in germline and other non-CNS tissues.

Appendix figure S6. Verification of *Mi-2* and *HDAC1* RNAi lines. qPCR measurement of non-neuronal genes in larval brains using alternative RNAi lines for *Mi-2* and *HDAC* (n = 3). These confirm the results obtained using the original RNAi lines. **P < 0.005, ***P < 0.0005 (one-tailed student's t-test). Error bars show standard deviation. Represented as mean ± SEM.

Appendix figure S7. Pupal lethality in NuRD component RNAi knockdown experiments. Percentage of pupae that die when NuRD subunits are knocked down in neurons (driven by *elav*-GAL4) during development. 3 independent experiments were performed for each genotype.

Appendix figure S8. GO analysis of down-regulated genes.

Appendix Figure S9. *Mi-2* knockdown does not affect NSC numbers in the VNC. A) Example images from ventral and dorsal sections of the VNC. Scale bars = 20 µm. B) Quantification of Dpn positive cells (no significant difference). 6 VNCs measured for each genotype. No significant difference (Student's t-test). Represented as a box plot.

Appendix figure S10. MTA1-like knockdown causes an optic lobe phenotype. A) Representative images of control (*elav-GAL4; ; mCherry RNAi*), and MTA1-like knockdown in the third instar larval CNS (all scale bars = 20 µm). Discs large (Dlg) = green, Deadpan (Dpn) = magenta. Neuroepithelial cells are highlighted by dashed lines. B) Quantification of optic lobe neuroepithelial cells of genotypes shown in panel A. At least 8 brains measured for each genotype. *** $p < 0.001$ (one-tailed student's t-test). Represented as a box plot.

Appendix figure S11. Larval crawl speed with *Mi-2* knockdown in NSCs. Larval crawl speed (cm/minute) in *wor*-GAL4 x *Mi-2* RNAi and *wor*-GAL4 x *mCherry* RNAi controls. No significant changes in crawl speed were observed (two-tailed students t-test, n = 10 animals per genotype). Represented as a box plot.

Appendix figure S12. Knockdown of *Mi-2* in adult brain neurons does not cause ectopic expression of genes. qPCR measurement of gene expression in adult heads. *Mi-2*^{RNAi} is induced for 24 hours using GAL80^{ts}. No significant changes in expression of either *vas, a10,* or *CG15446* were observed (one-tailed students t-test, represented as mean ± SEM.). 3 biological replicates per genotype.

Appendix figure S13. Optic lobe phenotype is not due to *Mi-2* knockdown in glial cells. A) Optic lobe of third instar larvae in which *repo*-GAL80 represses glial GAL4 expression. Loss of neuroepithelial cells is still observed as in *elav*-GAL4 *; Mi-2 RNAi* brains. Scale bar = 50 µm.

Appendix figure S14. The NE is present in *Mi-2 RNAi* 1st instar optic lobes. A) Characteristic rosette structure of the neuroepithelial cells in a control 1st instar optic lobe. B) and C) Characteristic rosette structures of the neuroepithelial cells in *elav*-GAL4 *; Mi-2 RNAi* 1st instar optic lobes. Scale bar = 20 µm.

References

Amaya, M., Desai, M., Gnanapragasam, M.N., Wang, S.Z., Zu Zhu, S., Williams, D.C., Jr., and Ginder, G.D. (2013). Mi2beta-mediated silencing of the fetal gamma-globin gene in adult erythroid cells. *Blood* ***121***, 3493-3501.

Arends, T., Dege, C., Bortnick, A., Danhorn, T., Knapp, J.R., Jia, H., Harmacek, L., Fleenor, C.J., Straign, D., Walton, K.*, et al.* (2019). CHD4 is essential for transcriptional repression and lineage progression in B lymphopoiesis. *Proc Natl Acad Sci U S A* ***116***, 10927-10936.

Aughey, G.N., Delandre, C., McMullen, J.P.D., Southall, T.D., and Marshall, O.J. (2021). FlyORF-TaDa allows rapid generation of new lines for in vivo cell-type-specific profiling of protein-DNA interactions in Drosophila melanogaster. *G3 (Bethesda)* ***11***.

Aughey, G.N., Estacio Gomez, A., Thomson, J., Yin, H., and Southall, T.D. (2018). CATaDa reveals global remodelling of chromatin accessibility during stem cell differentiation in vivo. *Elife* ***7***.

Bagni, C., Bray, S., Gogos, J.A., Kafatos, F.C., and Hsu, T. (2002). The Drosophila zinc finger transcription factor CF2 is a myogenic marker downstream of MEF2 during muscle development. *Mech Dev* ***117***, 265-268.

Berger, C., Renner, S., Luer, K., and Technau, G.M. (2007). The commonly used marker ELAV is transiently expressed in neuroblasts and glial cells in the Drosophila embryonic CNS. *Dev Dyn* ***236***, 3562-3568.

Bolte, S., and Cordelieres, F.P. (2006). A guided tour into subcellular colocalization analysis in light microscopy. *J Microsc* ***224***, 213-232.

Bornelov, S., Reynolds, N., Xenophontos, M., Gharbi, S., Johnstone, E., Floyd, R., Ralser, M., Signolet, J., Loos, R., Dietmann, S.*, et al.* (2018). The Nucleosome Remodeling and Deacetylation Complex Modulates Chromatin Structure at Sites of Active Transcription to Fine-Tune Gene Expression. *Mol Cell* ***71***, 56-72 e54.

Brehm, A., Langst, G., Kehle, J., Clapier, C.R., Imhof, A., Eberharter, A., Muller, J., and Becker, P.B. (2000). dMi-2 and ISWI chromatin remodelling factors have distinct nucleosome binding and mobilization properties. *EMBO J* ***19***, 4332-4341.

Burgold, T., Barber, M., Kloet, S., Cramard, J., Gharbi, S., Floyd, R., Kinoshita, M., Ralser, M., Vermeulen, M., Reynolds, N.*, et al.* (2019). The Nucleosome Remodelling and Deacetylation complex suppresses transcriptional noise during lineage commitment. *EMBO J* ***38***.

Dobin, A., Davis, C.A., Schlesinger, F., Drenkow, J., Zaleski, C., Jha, S., Batut, P., Chaisson, M., and Gingeras, T.R. (2013). STAR: ultrafast universal RNA-seq aligner. *Bioinformatics* ***29***, 15-21.

Eichler, K., Li, F., Litwin-Kumar, A., Park, Y., Andrade, I., Schneider-Mizell, C.M., Saumweber, T., Huser, A., Eschbach, C., Gerber, B.*, et al.* (2017). The complete connectome of a learning and memory centre in an insect brain. *Nature* ***548***, 175-182.

Estacio-Gomez, A., Hassan, A., Walmsley, E., Le, L.W., and Southall, T.D. (2020). Dynamic neurotransmitter specific transcription factor expression profiles during Drosophila development. *Biol Open* ***9***.

Favorov, A., Mularoni, L., Cope, L.M., Medvedeva, Y., Mironov, A.A., Makeev, V.J., and Wheelan, S.J. (2012). Exploring massive, genome scale datasets with the GenometriCorr package. *PLoS Comput Biol* ***8***, e1002529.

Filion, G.J., van Bemmel, J.G., Braunschweig, U., Talhout, W., Kind, J., Ward, L.D., Brugman, W., de Castro, I.J., Kerkhoven, R.M., Bussemaker, H.J.*, et al.* (2010). Systematic protein location mapping reveals five principal chromatin types in Drosophila cells. *Cell* ***143***, 212-224.

Gomez-Del Arco, P., Perdiguero, E., Yunes-Leites, P.S., Acin-Perez, R., Zeini, M., Garcia-Gomez, A., Sreenivasan, K., Jimenez-Alcazar, M., Segales, J., Lopez-Maderuelo, D.*, et al.* (2016). The Chromatin Remodeling Complex Chd4/NuRD Controls Striated Muscle Identity and Metabolic Homeostasis. *Cell Metab* ***23***, 881-892.

Hassan, A., Araguas Rodriguez, P., Heidmann, S.K., Walmsley, E.L., Aughey, G.N., and Southall, T.D. (2020). Condensin I subunit Cap-G is essential for proper gene expression during the maturation of post-mitotic neurons. *Elife* ***9***.

Herrmann, C., Van de Sande, B., Potier, D., and Aerts, S. (2012). i-cisTarget: an integrative genomics method for the prediction of regulatory features and cis-regulatory modules. *Nucleic Acids Res* ***40***, e114.

Ho, J.W., Jung, Y.L., Liu, T., Alver, B.H., Lee, S., Ikegami, K., Sohn, K.A., Minoda, A., Tolstorukov, M.Y., Appert, A.*, et al.* (2014). Comparative analysis of metazoan chromatin organization. *Nature* ***512***, 449-452.

Hoffmann, A., and Spengler, D. (2019). Chromatin Remodeling Complex NuRD in Neurodevelopment and Neurodevelopmental Disorders. *Front Genet* ***10***, 682.
Hsu, T., Bagni, C., Sutherland, J.D., and Kafatos, F.C. (1996). The transcriptional factor CF2 is a mediator of EGF-R-activated dorsoventral patterning in Drosophila oogenesis. *Genes Dev* ***10***, 1411-1421.
Hu, Y., Comjean, A., Perrimon, N., and Mohr, S.E. (2017). The Drosophila Gene Expression Tool (DGET) for expression analyses. *BMC Bioinformatics* ***18***, 98.
Huang, Z., and Kunes, S. (1996). Hedgehog, transmitted along retinal axons, triggers neurogenesis in the developing visual centers of the Drosophila brain. *Cell* ***86***, 411-422.
Janssens, J., Aibar, S., Taskiran, II, Ismail, J.N., Gomez, A.E., Aughey, G., Spanier, K.I., De Rop, F.V., Gonzalez-Blas, C.B., Dionne, M.*, et al.* (2022). Decoding gene regulation in the fly brain. *Nature*.
Jiao, W., Spreemann, G., Ruchti, E., Banerjee, S., Shi, Y., Stowers, R.S., Hess, K., and McCabe, B.D. (2021). Intact Drosophila Whole Brain Cellular Quantitation reveals Sexual Dimorphism. *bioRxiv*, 2021.2011.2003.467146.
Krause, S.A., Overend, G., Dow, J.A.T., and Leader, D.P. (2022). FlyAtlas 2 in 2022: enhancements to the Drosophila melanogaster expression atlas. *Nucleic Acids Res* ***50***, D1010-D1015.
Kreher, J., Kovac, K., Bouazoune, K., Macinkovic, I., Ernst, A.L., Engelen, E., Pahl, R., Finkernagel, F., Murawska, M., Ullah, I.*, et al.* (2017). EcR recruits dMi-2 and increases efficiency of dMi-2-mediated remodelling to constrain transcription of hormone-regulated genes. *Nat Commun* ***8***, 14806.
Kunert, N., Wagner, E., Murawska, M., Klinker, H., Kremmer, E., and Brehm, A. (2009). dMec: a novel Mi-2 chromatin remodelling complex involved in transcriptional repression. *EMBO J* ***28***, 533-544.
Liao, Y., Smyth, G.K., and Shi, W. (2019). The R package Rsubread is easier, faster, cheaper and better for alignment and quantification of RNA sequencing reads. *Nucleic Acids Res* ***47***, e47.
Love, M.I., Huber, W., and Anders, S. (2014). Moderated estimation of fold change and dispersion for RNA-seq data with DESeq2. *Genome Biol* ***15***, 550.
Low, J.K., Webb, S.R., Silva, A.P., Saathoff, H., Ryan, D.P., Torrado, M., Brofelth, M., Parker, B.L., Shepherd, N.E., and Mackay, J.P. (2016). CHD4 Is a Peripheral Component of the Nucleosome Remodeling and Deacetylase Complex. *J Biol Chem* ***291***, 15853-15866.
Marshall, O.J., and Brand, A.H. (2015). damidseq_pipeline: an automated pipeline for processing DamID sequencing datasets. *Bioinformatics* ***31***, 3371-3373.
Marshall, O.J., and Brand, A.H. (2017). Chromatin state changes during neural development revealed by in vivo cell-type specific profiling. *Nat Commun* ***8***, 2271.
Marshall, O.J., Southall, T.D., Cheetham, S.W., and Brand, A.H. (2016). Cell-type-specific profiling of protein-DNA interactions without cell isolation using targeted DamID with next-generation sequencing. *Nat Protoc* ***11***, 1586-1598.
Nichols, C.D., Becnel, J., and Pandey, U.B. (2012). Methods to assay Drosophila behavior. *J Vis Exp*.
Nitarska, J., Smith, J.G., Sherlock, W.T., Hillege, M.M., Nott, A., Barshop, W.D., Vashisht, A.A., Wohlschlegel, J.A., Mitter, R., and Riccio, A. (2016). A Functional Switch of NuRD Chromatin Remodeling Complex Subunits Regulates Mouse Cortical Development. *Cell Rep* ***17***, 1683-1698.
O'Shaughnessy-Kirwan, A., Signolet, J., Costello, I., Gharbi, S., and Hendrich, B. (2015). Constraint of gene expression by the chromatin remodelling protein CHD4 facilitates lineage specification. *Development* ***142***, 2586-2597.
Preissl, S., Fang, R., Huang, H., Zhao, Y., Raviram, R., Gorkin, D.U., Zhang, Y., Sos, B.C., Afzal, V., Dickel, D.E.*, et al.* (2018). Single-nucleus analysis of accessible chromatin in developing mouse forebrain reveals cell-type-specific transcriptional regulation. *Nat Neurosci* ***21***, 432-439.
Quinlan, A.R., and Hall, I.M. (2010). BEDTools: a flexible suite of utilities for comparing genomic features. *Bioinformatics* ***26***, 841-842.
Ragheb, R., Gharbi, S., Cramard, J., Ogundele, O., Kloet, S.L., Burgold, T., Vermeulen, M., Reynolds, N., and Hendrich, B. (2020). Differential regulation of lineage commitment in human and mouse primed pluripotent stem cells by the nucleosome remodelling and deacetylation complex. *Stem Cell Res* ***46***, 101867.
Rais, Y., Zviran, A., Geula, S., Gafni, O., Chomsky, E., Viukov, S., Mansour, A.A., Caspi, I., Krupalnik, V., Zerbib, M.*, et al.* (2013). Deterministic direct reprogramming of somatic cells to pluripotency. *Nature* ***502***, 65-70.

Ravenscroft, T.A., Janssens, J., Lee, P.T., Tepe, B., Marcogliese, P.C., Makhzami, S., Holmes, T.C., Aerts, S., and Bellen, H.J. (2020). Drosophila Voltage-Gated Sodium Channels Are Only Expressed in Active Neurons and Are Localized to Distal Axonal Initial Segment-like Domains. *J Neurosci **40***, 7999-8024.

Reddington, J.P., Garfield, D.A., Sigalova, O.M., Karabacak Calviello, A., Marco-Ferreres, R., Girardot, C., Viales, R.R., Degner, J.F., Ohler, U., and Furlong, E.E.M. (2020). Lineage-Resolved Enhancer and Promoter Usage during a Time Course of Embryogenesis. *Dev Cell **55***, 648-664 e649.

Reddy, B.A., Bajpe, P.K., Bassett, A., Moshkin, Y.M., Kozhevnikova, E., Bezstarosti, K., Demmers, J.A., Travers, A.A., and Verrijzer, C.P. (2010). Drosophila transcription factor Tramtrack69 binds MEP1 to recruit the chromatin remodeler NuRD. *Mol Cell Biol **30***, 5234-5244.

Rhee, D.Y., Cho, D.Y., Zhai, B., Slattery, M., Ma, L., Mintseris, J., Wong, C.Y., White, K.P., Celniker, S.E., Przytycka, T.M.*, et al.* (2014). Transcription factor networks in Drosophila melanogaster. *Cell Rep **8***, 2031-2043.

Selleck, S.B., and Steller, H. (1991). The influence of retinal innervation on neurogenesis in the first optic ganglion of Drosophila. *Neuron **6***, 83-99.

Southall, T.D., Davidson, C.M., Miller, C., Carr, A., and Brand, A.H. (2014). Dedifferentiation of neurons precedes tumor formation in Lola mutants. *Dev Cell **28***, 685-696.

Southall, T.D., Gold, K.S., Egger, B., Davidson, C.M., Caygill, E.E., Marshall, O.J., and Brand, A.H. (2013). Cell-type-specific profiling of gene expression and chromatin binding without cell isolation: assaying RNA Pol II occupancy in neural stem cells. *Dev Cell **26***, 101-112.

Tie, F., Furuyama, T., Prasad-Sinha, J., Jane, E., and Harte, P.J. (2001). The Drosophila Polycomb Group proteins ESC and E(Z) are present in a complex containing the histone-binding protein p55 and the histone deacetylase RPD3. *Development **128***, 275-286.

Tong, J.K., Hassig, C.A., Schnitzler, G.R., Kingston, R.E., and Schreiber, S.L. (1998). Chromatin deacetylation by an ATP-dependent nucleosome remodelling complex. *Nature **395***, 917-921.

Unhavaithaya, Y., Shin, T.H., Miliaras, N., Lee, J., Oyama, T., and Mello, C.C. (2002). MEP-1 and a homolog of the NURD complex component Mi-2 act together to maintain germline-soma distinctions in C. elegans. *Cell **111***, 991-1002.

Wade, P.A., Jones, P.L., Vermaak, D., and Wolffe, A.P. (1998). A multiple subunit Mi-2 histone deacetylase from Xenopus laevis cofractionates with an associated Snf2 superfamily ATPase. *Curr Biol **8***, 843-846.

Wang, H.B., and Zhang, Y. (2001). Mi2, an auto-antigen for dermatomyositis, is an ATP-dependent nucleosome remodeling factor. *Nucleic Acids Res **29***, 2517-2521.

Wang, Z., Zang, C., Cui, K., Schones, D.E., Barski, A., Peng, W., and Zhao, K. (2009). Genome-wide mapping of HATs and HDACs reveals distinct functions in active and inactive genes. *Cell **138***, 1019-1031.

Xue, Y., Wong, J., Moreno, G.T., Young, M.K., Cote, J., and Wang, W. (1998). NURD, a novel complex with both ATP-dependent chromatin-remodeling and histone deacetylase activities. *Mol Cell **2***, 851-861.

Yamada, T., Yang, Y., Hemberg, M., Yoshida, T., Cho, H.Y., Murphy, J.P., Fioravante, D., Regehr, W.G., Gygi, S.P., Georgopoulos, K.*, et al.* (2014). Promoter decommissioning by the NuRD chromatin remodeling complex triggers synaptic connectivity in the mammalian brain. *Neuron **83***, 122-134.

Yoshida, T., Hazan, I., Zhang, J., Ng, S.Y., Naito, T., Snippert, H.J., Heller, E.J., Qi, X., Lawton, L.N., Williams, C.J.*, et al.* (2008). The role of the chromatin remodeler Mi-2beta in hematopoietic stem cell self-renewal and multilineage differentiation. *Genes Dev **22***, 1174-1189.

Zacharioudaki, E., Falo Sanjuan, J., and Bray, S. (2019). Mi-2/NuRD complex protects stem cell progeny from mitogenic Notch signaling. *Elife **8***.

Zhang, W., Aubert, A., Gomez de Segura, J.M., Karuppasamy, M., Basu, S., Murthy, A.S., Diamante, A., Drury, T.A., Balmer, J., Cramard, J.*, et al.* (2016). The Nucleosome Remodeling and Deacetylase Complex NuRD Is Built from Preformed Catalytically Active Sub-modules. *J Mol Biol **428***, 2931-2942.

Zhang, Y., LeRoy, G., Seelig, H.P., Lane, W.S., and Reinberg, D. (1998). The dermatomyositis-specific autoantigen Mi2 is a component of a complex containing histone deacetylase and nucleosome remodeling activities. *Cell **95***, 279-289.

Ziffra, R.S., Kim, C.N., Ross, J.M., Wilfert, A., Turner, T.N., Haeussler, M., Casella, A.M., Przytycki, P.F., Keough, K.C., Shin, D.*, et al.* (2021). Single-cell epigenomics reveals mechanisms of human cortical development. *Nature **598***, 205-213.